Current Nanoscience, 2018, *14*, 54-61

RESEARCH ARTICLE

Early Stages of Antibacterial Damage of Metallic Nanoparticles by TEM and STEM-HAADF

Beatriz Liliana España-Sánchez[a,b], Carlos Alberto Ávila-Orta[a,*], Luis Felipe Padilla-Vaca[c,*], Enrique Díaz Barriga-Castro[a], Florentino Soriano-Corral[a], Pablo González-Morones[a], Diana Guadalupe Ramírez-Wong[b] and Gabriel Luna-Bárcenas[b]

[a]*Departamento de Materiales Avanzados, Centro de Investigación en Química Aplicada (CIQA), Blvd. Enrique Reyna Hermosillo No. 140, Saltillo, Coahuila 25294, México;* [b]*Centro de Investigación y de Estudios Avanzados del Instituto Politécnico Nacional (CINVESTAV) Unidad Querétaro. Libramiento Norponiente No. 2000, Fracc. Real de Juriquilla. Querétaro, Querétaro, 76230, México;* [c]*Departamento de Biología, División de Ciencias Naturales y Exactas, Universidad de Guanajuato. Noria Alta s/n, Guanajuato, Guanajuato 36050, México*

ARTICLE HISTORY

Received: March 27, 2017
Revised: May 24, 2017
Accepted: August 23, 2017

DOI:
10.2174/2468187307666170906150731

Abstract: ***Background*:** Propagation of pathogens has considered an important health care problem due to their resistance against conventional antibiotics. The recent challenge involves the design of functional alternatives such as nanomaterials, used as antibacterial agents. Early stages of antibacterial damage caused by metallic nanoparticles (NPs) were studied by Transmission Electron Microscopy (TEM) and combined Scanning Transmission Electron Microscopy with High Angle Annular Dark Field (STEM-HAADF), aiming to contribute to the elucidation of the primary antibacterial mechanism of metallic NPs.

***Methods*:** We analyze the NPs morphology by TEM and their antibacterial activity (AA) with different amounts of Ag and Cu NPs. Cultured *P. aeruginosa* were interacted with both NPs and processed by TEM imaging to determine NPs adhesion into bacteria wall. Samples were analyzed by combined STEM-HAADF to determine the NPs penetration into bacterium and elemental mapping were done.

***Results*:** Both NPs displays AA depending on NPs concentration. TEM images show NPs adhesion on bacterial cells, which produces morphological changes in the structure of the bacteria. STEM-HAADF also proves the NPs adhesion and penetration by intracellular localization, detecting Ag/Cu species analyzed by elemental mapping. Moreover, the relative amount of phosphorus (P) and sulfur (S) increases slightly in *P. aeruginosa* with the presence of NPs. These elements are associated with damaged proteins of the outer cell membrane.

***Conclusions*:** Combined microscopy analyses suggest that the early stages of antibacterial damage caused by alteration of bacterial cell wall, and can be considered a powerful tool aiming to understand the primary antibacterial mechanism of NPs.

Keywords: Antibacterial damage, metallic nanoparticles, silver, copper, HRTEM, STEM-HAADF.

1. INTRODUCTION

Propagation of pathogens and their antimicrobial resistance against conventional antibiotics have generated scientific interest, aiming to design effective and low-cost alternatives to prevent infectious diseases [1, 2]. Recently, metallic nanoparticles (NPs) have demonstrated high bacteriostatic and bactericidal properties associated with the increase of surface area to volume ratio, enhancing their physical and chemical activity, and they are considered as the new generation of antimicrobial agents [3, 4]. It is well known that silver (Ag) and copper (Cu) NPs present high antimicrobial properties in contact with microorganisms, and have an emerging use in medical devices and health care applications [5-7]. Several studies have been focused on the antimicrobial properties of metallic NPs and their action mechanism in contact with microorganisms, but is still not well understood [8, 9]. Different bacterial damage processes have been reported, and they are associated with alterations to different cellular components, such as cell wall [10], proteins [11] and DNA [12]. All of them induce changes in cell function to finally promote cell death.

Bactericidal properties derived from NPs, have been linked to different factors, such as NPs composition and morphology [13, 14], metallic ions released by the NPs sur-

*Address correspondence to these authors at the Departamento de Materiales Avanzados, Centro de Investigación en Química Aplicada (CIQA), Blvd. Enrique Reyna Hermosillo No. 140, Saltillo, Coahuila 25294, México; Tel: (844) 4389830 ext. 1391;
E-mail: carlos.avila@ciqa.edu.mx
Departamento de Biología, División de Ciencias Naturales y Exactas, Universidad de Guanajuato. Noria Alta s/n, Guanajuato, Guanajuato 36050, México; Tel: (477) 7320006 ext. 8166; E-mail: padillaf@ugto.mx

1875-6786/18 $58.00+.00

face [15, 16], NPs concentration [17], and the structural composition of bacterial cell [18]. In this regard, Transmission Electron Microscopy (TEM) is a useful technique for nanomaterials characterization, since it allows to observe size, shape, structure, and material dispersion at the nanoscale [19]. Recent advances in electron microscopy offer new analytical techniques based on the image contrast and their correlation with the atomic mass, allowing to determine morphology and composition. The implementation of High Angle Annular Dark Field (HAADF) has made important developments in NPs analyses [20]. The progress of combined STEM-HAADF technique is related with the imaging of biological samples morphology and its elemental analysis at nanometric scale. A major challenge of combined techniques is the analyses of bacterial damage produced by the interaction with NPs, aiming to elucidate the early stages of the process.

The present study is focused on the antibacterial damage produced by the interaction of Ag and Cu NPs with Gram-negative *Pseudomonas aeruginosa* by means of TEM and combined STEM-HAADF. In this regard, NPs morphology and their antibacterial activity (AA) were determined. The adhesion and penetration of NPs were determined by TEM and STEM-HAADF, aiming to contribute to the elucidation of the primary antibacterial mechanism of metallic NPs.

2. MATERIALS AND METHODS

2.1. Materials

Spherical silver (Ag, 20-30 nm) and copper (Cu, 25 nm) NPs were purchased from SkySpring Nanomaterials Inc., and used as received. Bactericidal assays were done using *Pseudomonas aeruginosa* ATCC #13388 from American Type Culture Collection. Bacterium was growth in Luria Bertani broth (LB) purchased from BD Bioxon. Sterile phosphate saline buffer (PBS) with Tween 80 at 1% was prepared for NPs dispersion before their interaction with bacterium. Sodium cacodylate, osmium tetraoxide, epoxic resin EPON 810 and dimethyl phthalate (DMP) for bacterial sample preparation from TEM were purchased from Electron Microscopy Sciences.

2.2. NPs Characterization and Antibacterial Activity (AA)

Ag and Cu NPs (200 µg/mL) suspended in ethanol was diluted 1:4 and sonicated during 10 minutes. A droplet of each suspension was placed in copper (for Ag NPs) and nickel (for Cu NPs) grids at 300 mesh coated with lacey carbon, respectively. NPs were characterized by TEM and STEM, and processed by fast Fourier transform (FFT) for crystalline structure, using an electron microscope FEI-TITAN with 200 kV of accelerating voltage. The NPs size distribution was calculated by image analysis using the software ImageJ®. The analysis was done counting the average of five representative TEM images of Ag and Cu (*ca.* 300 for Ag and 500 for Cu NPs), respectively. X ray diffraction measurements (XRD) were done in a diffractometer Siemens D5000 in reflection mode, at 35 kV, with a filament intensity of 25 mA, ranging from 20 to 80 in 2θ at 0.1°/min, using a copper lamp. AA of NPs were determined using an inoculum of $1x10^5$ CFU/mL of *P. aeruginosa* grown in LB broth at 37°C during 16 h. NPs suspensions (25, 50, 100, 200, 400, 800 and 1600 µg/mL) were prepared in PBS/Tween 80 buffer and sonicated during 2 minutes at 70% amplitude. An equal volume from bacterial/NPs suspension was placed in sterile eppendorf tubes and mixed during 1 h at 37°C. Subsequently, an aliquot of each suspension was plated in LB agar and incubated at 37°C during 16 h. The AA was calculated according to the equation [21]:

Antibacterial Activity (AA) % = (Co-C/Co) x 100

Where *Co* is the number of bacterial colonies in the control without NPs, and *C* is the survival bacterial colonies after interaction with NPs.

2.3. Electron Microscopy Characterization

Bacteria was brought in contact with Ag or Cu NPs during 1 h, and then prepared for conventional TEM. Cells were collected by centrifugation at 6000 rpm during 2 minutes, washed with sterile PBS and supernatant was removed. Glutaraldehyde (1 mL, 2%) was placed in each sample during 1 h for prefixing and washed with sodium cacodylate buffer. Samples were stained with osmium tetraoxide 1% during 2 h. Dehydration of cells was carried out using ethanol 50, 70, 96 and 100%, respectively. Subsequently, each sample was fixed in epoxic resin EPON 810 with DMP and polymerized at 60°C during 48 h. Fixed samples were cut in a Leica ultramicrotome with an average thickness of 70 nm, and placed on a copper (bacteria/Ag NPs) or nickel (bacteria/Cu NPs) grid, accordingly. The bacterial morphology and microstructure were examined by conventional TEM, STEM and combined STEM-HAADF using a FEI-TITAN microscopy at 80-300 kV, operated at accelerating voltage of 200 kV.

3. RESULTS

First, commercially available Ag and Cu NPs were characterized as received. Transmission Electron Microscopy (TEM) images show spherical Ag NPs (Fig. **1a**), with an average size of 10-30 nm and semi-spherical Cu NPs of 60 nm (Fig. **1b**). Whereas Cu NPs are larger than the value specified by the suppliers (25 nm), we observe clusters of Ag and Cu NPs that might be attributed to their high surface energy. Moreover, the selected area of electron diffraction (SAED) patterns for Ag NPs show the characteristic crystalline planes of metallic Ag. XRD analysis reveal four peaks located at 2θ 38.03, 44.20, 64.45 and 77.37°, corresponding to crystalline planes (111), (200), (220) and (311), associated to the FCC structure of silver [22].On the other hand, XRD confirms the presence of elemental Cu (Fig. **1b**) located at 2θ 43.47, 50.58 and 74.29°, which correspond to crystalline planes (111), (200) and (220) [23]. Also, Cu_2O is detected by XRD, located in 2θ 37.81° (111) and 61.69° (220), suggesting that partial oxidation of Cu NPs takes place on the surface of the particles due to the air exposition.

In a second step, the antibacterial activity (AA) of Ag and Cu NPs was evaluated against Gram-negative bacteria *P. aeruginosa.* Quantitative results of AA after 1 hour contact between the bacteria and a range of NPs concentrations are presented in Fig. (**2**). It is clear that the bactericidal effect

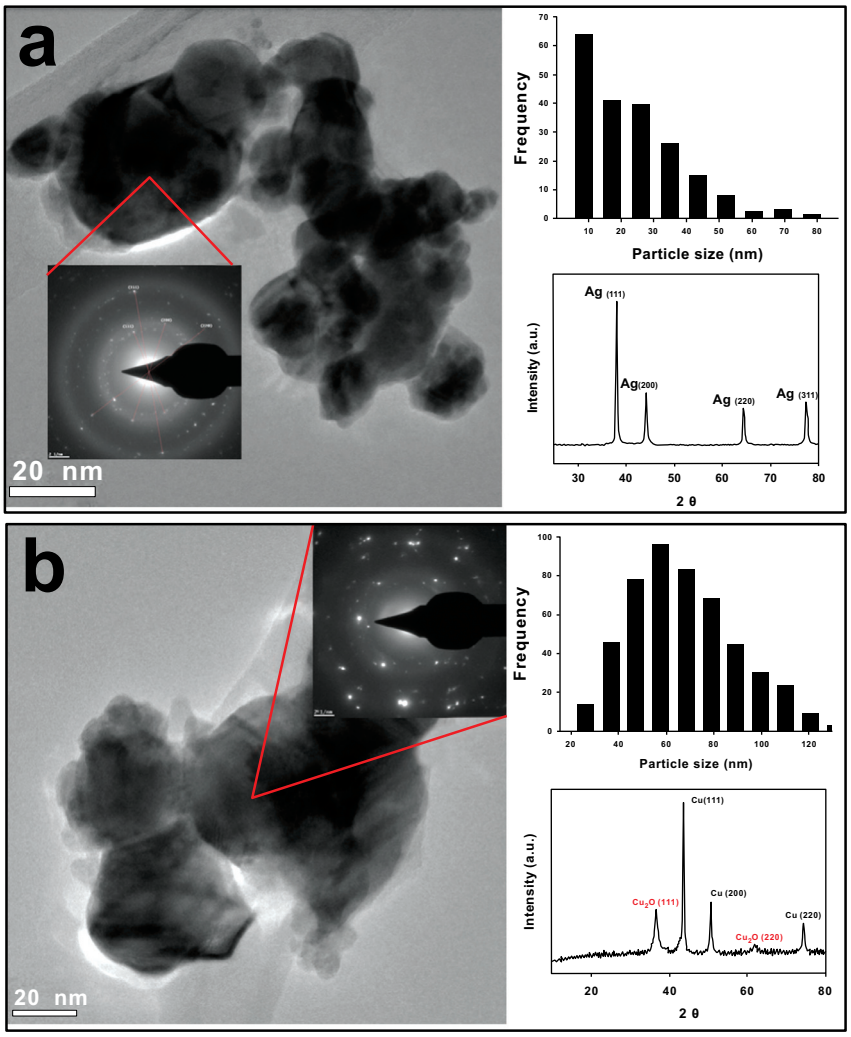

Fig. (1). TEM images of commercial NPs as received. **a**) Ag NPs and **b**) Cu NPs. Upper right histogram and lower right XRD. Ag NPs present an average size of 10-30 nm and spherical morphology. Cu NPs shows an average size of 60 nm and semi-spherical morphology. A thin coating of Cu_2O is detected, associated with a partial oxidation of Cu NPs exposed to air.

after 1 h of incubation depends on NPs concentration for both NPs, a result in agreement with Mukhherji's work [17]. In the concentrations spanning from 25 to 800 µg/mL Ag NPs exhibit lower AA compared to Cu NPs from 25 to 800 µg/mL, reaching up to 60% of AA at 800 µg/mL. Also, Cu NPs already have *ca.* 80% AA at 200 µg/mL, and entirely inhibit bacterial growth from 400 µg/mL. Nonetheless, both NPs exhibit 100% AA at the highest concentration (1600 µg/mL). It is to noteworthy to mention that we do not observe any evidence of bacterial inhibition produced by NPs after bacterium plating.

To continue our study, we followed the interaction of *P. aeruginosa* with Ag and Cu NPs by TEM imaging (Fig. **3**). Aiming to compare the early stage of antibacterial damage, we chose 400 and 100 µg/mL of Ag and Cu NPs, respectively (which in turn produce 35 and 42% of AA, accordingly). Fig. (**3a**) presents *P.* aeruginosa before any NPs interaction, a typical morphology is observed with an average size of 1.45 x 0.5 µm [24]. A characteristic thin cell wall

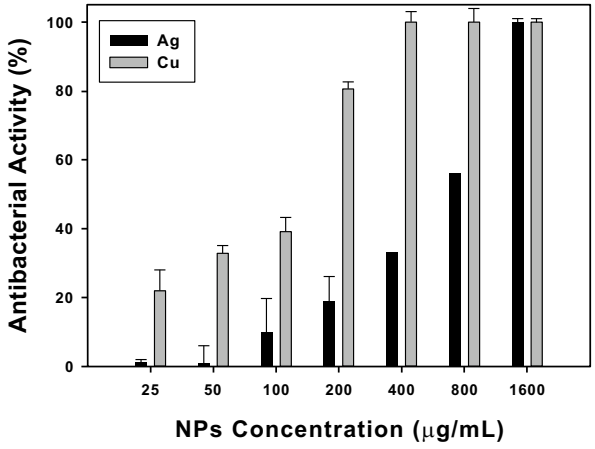

Fig. (2). Antibacterial activity (AA) of Ag and Cu NPs against Gram-negative *P. aeruginosa* at 37°C during 1 h. The bactericidal effect depends of NPs concentration. Ag NPs shows lower AA compared to Cu NPs.

with an average thickness of 40 nm was observed, common for Gram-negative bacteria [25]. Then, Fig. (**3b**) shows *P. aeruginosa* with Ag NPs, and while Fig. (**3c**) displays the bacteria with Cu NPs. In both cases, it was observed that NPs adhere on and penetrate the cell wall. Moreover, the bacteria that are in direct contact with NPs (arrows) present some alterations in their cellular structure.

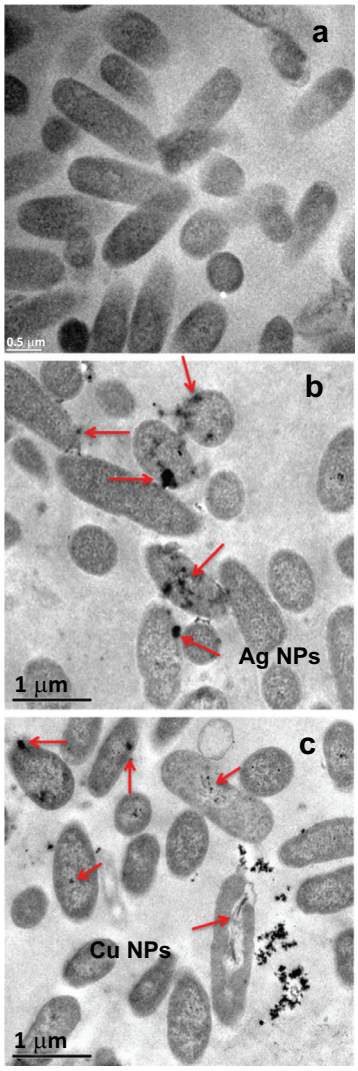

Fig. (3). TEM images of *P. aeruginosa* suspended in LB media after 1 h. **a**) control, **b**) interaction with 400 µg/mL of Ag NPs and **c**) interaction with 100 µg/mL of Cu NPs. It can be seen the presence of Cu and Ag NPs (arrows) in contact with *P. aeruginosa*.

Thus, we use HRTEM to go one step closer to the interaction between *P. aeruginosa* with Ag and Cu NPs (Fig. **4**). Fig. (**4a**) shows the cross section of a bacterium in contact with 400 µg/mL of Ag NPs. We observe the presence of NPs agglomerates around the bacterial wall, and the defined NPs of 20 nm. The cell wall is distorted by the Ag NPs (arrows), which seem to finally lead to NPs internalization. Similarly, 100 µg/mL of Cu NPs were brought in contact with *P. aeruginosa*. Fig. (**4b**) shows Cu NPs are trapped in the bacterial wall. Equally important to point out here, Cu NPs inside the cell have an average size of 30 nm and their morphology is

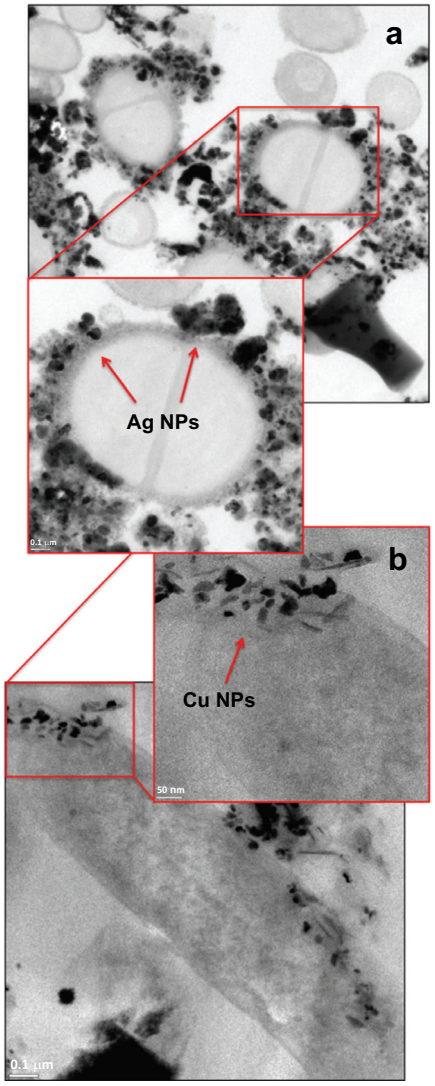

Fig. (4). HRTEM images of cross section of *P. aeruginosa* in contact with **a**) Ag NPs and **b**) Cu NPs during 1 h at 37°C. Alteration in bacterial structure and damaged cell wall is observed by NPs adhesion and penetration.

not dominantly semi-spherical. The latter phenomena is probably associated to the partial dissolution of Cu^{2+} ions in liquid media [26] associated to the oxide layer, and will be discussed later on.

Finally, we perfomed combined STEM-HAADF analyses to confirm that these NPs inside *P. aeruginosa* correspond to the our metallic nanomaterials. A qualitative mapping of Ag and Cu is done therefore. Additionally, phosphorus (P) and sulfur (S) elements are mapped since both are important components of bacterial cell wall. In Fig. (**5**), we observe the STEM-HAADF image of *P. aeruginosa* and its elemental maps prior to the addition of NPs. The smal frames on top show an extremely low concentration of Ag and Cu. In particular, the presence of Ag may be attributed for the detection limit for the equipment, while Cu may be linked to common metallic traces that result of the bacterial metabolic process [27]. The bottom frames in Fig. (**5**) display a rich P

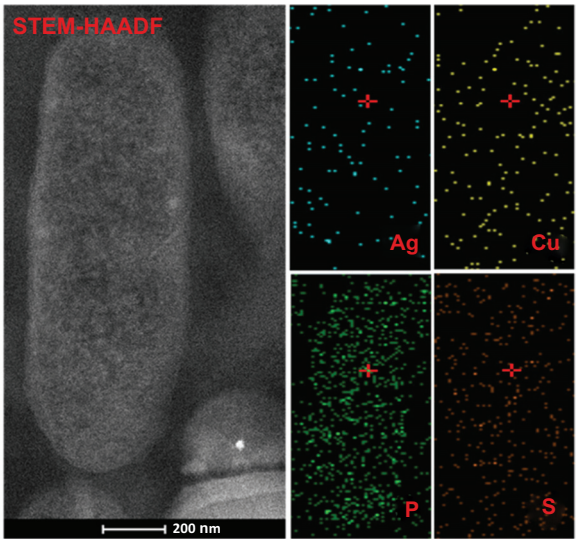

Fig. (5). STEM-HAADF image and elemental mapping of *P. aeruginosa*. Bacterial cross section shows the morphological characteristics of bacterial structure. Qualitative elemental mapping show low concentration of Cu species associated with common metal levels located inside bacteria. P and S elements present are associated with the elemental bacterial composition.

and S inside the cell. Both elements are regularly distributed, since they are components of the lipids, proteins and nuclei acids in the bacteria [28].

Fig. (**6**) displays STEM-HAADF images and elemental mapping of *P. aeruginosa* with Ag NPs (400 µg/mL, top) and Cu NPs (100 µg/mL, bottom). Fig. (**6a**) shows that Ag NPs are around the bacterial wall and penetrated into bacterial cytoplasm (arrows). When we subtract the Ag content on Figs. (**5** and **6**) (before and after NPs interaction) we found an increase of *ca*. 30% in Ag species after the NPs exposure. According to the AA assay (Fig. **2**), 400 µg/mL of Ag NPs decreases bacterial activity by 42%. Therefore, the adhesion and penetration of this amount of Ag NPs seems to inhibit bacterial growth. Following the same method of subtraction for P and S elements, we calculate an increase of *ca.* 60% with a change of distribution of both components. The later might be linked to the interaction between NPs and proteins of the outer membrane. The increase of P elements can be associated with the possible repair mechanism of phospholipidic structure of bacteria [29]. In parallel, the interaction of *P. aeruginosa* with Cu NPs (100 µ g/mL) was analyzed by STEM-HAADF (Fig. **6b**). The left image shows Cu NPs well dispersed in the cell structure (arrows), presenting an increase of *ca*. 15% of Cu species, and an increase of *ca*. 20% in P and S concentration, if compared with the untreated bacterium (Fig. **5**). In both cases, STEM-HAADF images provide evidence of NPs penetration into the bacteria, while elemental mapping shows a slight increase in metal species.

4. DISCUSSION

Ag and Cu NPs have emerged as relevant materials for the synthesis of biomedical devices due to their antibacterial

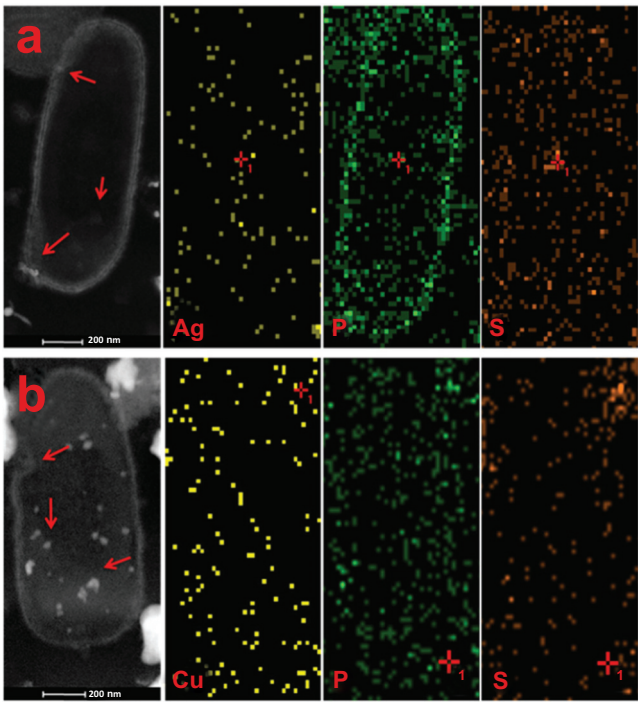

Fig. (6). STEM-HAADF image and elemental mapping of Ag, Cu, P and S in *P. aeruginosa* interacted with **a**) Ag NPs and **b**) Cu NPs. It can be seen the presence of Ag/Cu species distributed all throughout the cell (arrows), producing the adhesion and penetration of NPs. Moreover, P and S elements have been increased by the presence of NPs.

properties. Here, we go into a detailed observation of the early stages of AA produced by Ag and Cu NPs using commercial sources. Therefore, we first evaluated the chemical composition and morphology of the received NPs. TEM images confirm that Ag and Cu NPs are well in the nano scale range (Fig. **1**), as reported previously [21]. From the XRD we interpret that Ag are pure but Cu NPs are partially oxidized. Nonetheless, other authors have reported that Cu NPS hold their antibacterial properties besides a thin layer of oxide [30, 31].

The bactericidal properties (AA) of Ag and Cu NPs were corroborated and contrasted against *P. aeruginosa* as a model bacteria (Fig. **2**). In the range of concentrations presented, both types of NPs reach their full AA. Although, higher concentrations of Ag NPs are required to have a comparable effect with Cu NPs. It has been reported that Cu NPs and its oxides have high antibacterial effect associated with the release of Cu^{2+} ions in solution and its feasibility to reach to the bacterial outer membrane [17, 32]. Moreover, we should bear in mind that the sensitivity of bacteria towards NPs concentration varies according to the microbial species [17].

To observe the early antibacterial damage caused by NPs in *P. aeruginosa*, we use different electron microscopy techniques. First, our TEM images (Fig. **3**) suggest that the interaction between bacteria and NPs induce changes in bacterial

structure as the overall shape becomes irregular and the cell wall is distorted after direct contact. Metallic NPs and other ionic species that they might release from their surface when in solution could interact with the anionic lipopolysaccharides of Gram-negative cell wall, as it has been reported before [33, 34]. These interactions then, lead to the disequilibrium on the cell causing permeation and resulting finally in cell death [35, 36]. However, in our early stages AA micrographs, the combined effect of NPs and ion release did not produce the complete rupture of the outer membrane of bacteria [37, 38].

Yet, HRTEM allowed us to clearly identify NPs adhesion and embedding on the cell wall (Fig. **4**). This observation becomes relevant when we consider that bacterial cell wall properties play a crucial role in NPs diffusion [18, 39]. Following this principle and our observations of the cross section of bacterium, we believe that the cell wall alterations might lead to a better diffusion of more NPs and finally to cell death. In fact, a more noticeable NPs adhesion and penetration is detected in Fig. (**4b**), and Cu NPs achieve AA at lower concentrations. In this regard, HRTEM resolution is a valuable tool to elucidate the primary mechanism of metallic NPs.

It is important to note that different NPs concentrations (between Ag and Cu) were chosen to achieve significantly similar AA after 1 h (400 µg/mL of Ag NPs and 100 µg/mL of Cu NPs). Indeed, Cu NPs have better antibacterial properties compared with Ag NPs. We think that the improved AA of Cu NPs, results from the combined effect of Cu NPs and Cu^{2+}/CuO species that form in liquid media after, Cu NPs dispersion. This phenomena is called the "Trojan horse effect" which involves the NPs dispersion and oxide layer solubilisation in the culture medium and inside the cells [40, 41]. The synergistic effect of penetrated NPs and ions might induce cytotoxicity by the production of reactive oxygen species (ROS), with subsequent alteration in respiratory chain and DNA replication, to finally induce cellular death [42-45].

HAADF technique is generated for the electron that have been scattered at high angles, producing an image with high contrast related with the differences of atomic number (Z) between organic/inorganic phases, and it is considered a powerful tool to evaluate nano-sized metallic NPs embedded on organic substrates [46]. Therefore, we use it to corroborate the Ag and Cu NPs adhesion and penetration on *P. aeruginosa*. STEM-HAADF image and qualitative mapping of Ag and Cu, (Fig. **6**) show NPs distributed within the bacteria and on the wall. Moreover, the slight increase and redistribution of P and S elements propose the possible phospholipid and protein damage produced by the interaction of NPs with the specific adsorption sites regularly distributed on the lipopolysaccharidic outer cell of Gram-negative *P. aeruginosa* [47-49].

Some authors have suggested the bactericidal mechanism of Ag NPs, based on the electrostatic attraction between Ag^{+} ions (on the surface of Ag NPs) and the negative charges present on the cell membrane, which is key to produce alterations of cell permeability [50, 51]. Under this criteria, Lok *et al.* [11] proposed that Ag NPs can induce the collapse of *E. coli* plasma membrane and cell death later on. Other authors suggest that the NPs concentration and their interaction with microorganisms is critical to produce the formation of holes of "pits", altering the elemental cell function [35, 46, 52]. In both cases, the combined effect of adhesion and penetration process produced by ions and NPs is crucial to produce a cytotoxic effect [47]. The novelty of this work is to visualize the early stages of antibacterial damage produced by metallic NPs by the use of combined HRTEM and STEM-HAADF, paving the way to better understand the bactericidal primary mechanism of Ag and Cu NPs. We believe that our results contribute in the rational design of novel antimicrobial nanomaterials.

CONCLUSION

This study shows the early stages of antibacterial damage caused by metallic NPs on Gram-negative *Pseudomonas aeruginosa* by means of HRTEM and combined STEM-HAADF. Commercial NPs were in nano size range and present antibacterial activity as a function of NPs concentration and chemistry. Cu NPs are more effective than Ag NPs. In the early stages of antibacterial damage, the bacteria/NPs interaction in liquid media produces the NPs adhesion into bacterial wall, resulting in important changes of cellular structure. STEM-HAADF images corroborates the NPs penetration inside bacteria, producing an increase of Ag/Cu species with P and S elements, main components of biomolecules in the bacterial cell. This behavior suggest that protein damage is produced by the interaction of NPs with the specific adsorption sites regularly distributed on the lipopolysaccharidic outer cell. Combined analyses of TEM and STEM-HAADF can be a powerful tool to understand the primary antibacterial mechanism of metallic NPs and the bacterial response to damage, which are key for the rational design of antimicrobial nanomaterials.

LIST OF ABBREVIATIONS

AA	=	Antibacterial activity
Ag	=	Silver
Cu	=	Copper
HRTEM	=	High Resolution Transmission Electron Microscopy
NPs	=	Metallic nanoparticles
P	=	Phosphorous
S	=	Sulfur
STEM-HAADF	=	Scanning Transmission Electron Microscopy with High Angle Annular Dark Field
TEM	=	Transmission Electron Microscopy.

ETHICS APPROVAL AND CONSENT TO PARTICIPATE

Not applicable.

HUMAN AND ANIMAL RIGHTS

No Animals/Humans were used for studies that are base of this research.

CONSENT FOR PUBLICATION

Not applicable.

CONFLICT OF INTEREST

The authors declare no conflict of interest, financial or otherwise.

ACKNOWLEDGEMENTS

The authors wish to thank the financial support to CONACYT through project 127151. Thanks to Jannet Anaid Valdéz-Garza, Silvia-Torres-Rincón, Lourdes Palma-Tirado, Ángeles Rangel-Serrano and Itzel Páramo-Pérez for their technical support.

B.L. España-Sánchez, F. Padilla-Vaca and C. Ávila-Orta contributed to conceived, design experiments and analysis of data. B.L. España-Sánchez and E. Díaz Barriga-Castro and F. Soriano-Corral contributed to perform the experiments. P. González-Morones, D. Ramírez-Wong and G. Luna-Bárcenas contributed to materials and analysis of results. All authors contributed to writing and revision of manuscript.

REFERENCES

[1] Zazo, H.; Colino, C.I.; Lanao, J.M. Current applications of nanoparticles in infectious diseases. *J. Control. Release,* **2016**, *224*, 86-102.

[2] Gupta, A.; Landis, R.F.; Rotello, V.M. Nanoparticle-based antimicrobials: surface functionality is critical. *F1000Research,* **2016**, *5,* doi: 10.12688/f1000research.7595.1.

[3] Rai, M.; Yadav, A.; Gade, A. Silver nanoparticles as a new generation of antimicrobials. *Biotechnol. Adv.,* **2009**, *27*, 76-83.

[4] Seil, J.T.; Webster, T.J. Antimicrobial applications of nanotechnology: Methods and literature. *Int. J. Nanomed.,* **2012**, *7*, 2767-2781.

[5] Burgess, R. Medical applications of nanoparticles and nanomaterials. *Stud. Health Technol. Inform.,* **2009**, *149*, 257-283.

[6] Villanueva, M.E.; Diez, A.M.; González, J.A.; Pérez, C.J.; Orrego, M.; Piehl, L.; Teves, S.; Copello, G.J. Antimicrobial activity of starch hydrogel incorporated with copper nanoparticles. *ACS Appl. Mater. Interfaces*., **2016**, *8*(25), 16280-16288.

[7] Panáček, A.; Smékalová, M.; Večeřová, R.; Bogdanová, K.; Röderová, M.; Kolář, M.; Kilianová, M.; Hradilová, Š.; Froning, J. P.; Havrdová, M.; Prucek, R.; Zbořil, R.; Kvítek, L. Silver nanoparticles strongly enhance and restore bactericidal activity of inactive antibiotics against multiresistant enterobacteriaceae. *Colloids Surf. B Biointerfaces*., **2016**, *142*, 392-399.

[8] Ingle, A.P.; Duran, N.; Rai, M. Bioactivity, mechanism of action, and cytotoxicity of copper-based nanoparticles: A review. *Appl. Microbiol. Biotechnol.,* **2014**, *98*, 1001-1009.

[9] Kon, K.; Rai, M. Metallic nanoparticles: Mechanism of antibacterial action and influencing factors. *J. Comp. Clin. Pathol. Res.,* **2013**, *2*, 160-174.

[10] Karlsson, H.L.; Cronholm, P.; Hedberg, Y.; Tornberg, M.; De Battice, L.; Svedhem, S.; Wallinder, I.O. Cell membrane damage and protein interaction induced by copper containing nanoparticles--importance of the metal release process. *Toxicology,* **2013**, *313*, 59-69.

[11] Lok, C.-N.; Ho, C.-M.; Chen, R.; He, Q.-Y.; Yu, W.-Y.; Sun, H.; Tam, P.K.-H.; Chiu, J.-F.; Che, C.-M. Proteomic analysis of the mode of antibacterial action of silver nanoparticles. *J. Proteome Res.,* **2006**, *5*, 916-924.

[12] Rim, K.-T.; Song, S.-W.; Kim, H.-Y. Oxidative DNA damage from nanoparticle exposure and its application to workers' health: A literature review. *Saf. Health Work,* **2013**, *4*, 177-186.

[13] Lu, Z.; Rong, K.; Li, J.; Yang, H.; Chen, R. Size-dependent antibacterial activities of silver nanoparticles against oral anaerobic pathogenic bacteria. *J. Mater. Sci. Mater. Med.,* **2013**, *24*, 1465-1471.

[14] Pal, S.; Tak, Y.K.; Song, J.M. Does the antibacterial activity of silver nanoparticles depend on the shape of the nanoparticle? A study of the gram-negative bacterium *Escherichia coli*. *Appl. Environ. Microbiol.,* **2007**, *73*, 1712-1720.

[15] Xiu, Z.; Zhang, Q.; Puppala, H.L.; Colvin, V.L.; Alvarez, P.J.J. Negligible particle-specific antibacterial activity of silver nanoparticles. *Nano Lett.,* **2012**, *12*, 4271-4275.

[16] Kittler, S.; Greulich, C.; Diendorf, J.; Köller, M.; Epple, M. Toxicity of silver nanoparticles increases during storage because of slow dissolution under release of silver ions. *Chem. Mater.,* **2010**, *22*, 4548-4554.

[17] Ruparelia, J.P.; Chatterjee, A.K.; Duttagupta, S.P.; Mukherji, S. Strain specificity in antimicrobial activity of silver and copper nanoparticles. *Acta Biomater.,* **2008**, *4*, 707-716.

[18] Hajipour, M.J.; Fromm, K.M.; Ashkarran, A.A.; Jimenez de Aberasturi, D.; de Larramendi, I.R.; Rojo, T.; Serpooshan, V.; Parak, W.J.; Mahmoudi, M. Antibacterial properties of nanoparticles. *Trends Biotechnol.,* **2012**, *30*, 499-511.

[19] Neogy, S.; Savalia, R.T.; Tewari, R.; Srivastava, D.; Dey, G.K. Transmission electron microscopy of nanomaterials. *Indina J. Pure Ap. Phy*., **2006**, *44*(2),119-124.

[20] Utsunomiya, S.; Ewing, R.C. Application of high-angle annular dark field scanning transmission electron microscopy, scanning transmission electron microscopy-energy dispersive x-ray spectrometry, and energy-filtered transmission electron microscopy to the characterization of nanopar. *Environ. Sci. Technol.,* **2003**, *37*, 786-791.

[21] España-Sánchez, B.L.; Ávila-Orta, C.A.; Padilla-Vaca, F.; Neira-Velázquez, M.G.; González-Morones, P.; Rodríguez-González, J.A.; Hernández-Hernández, E.; Rangel-Serrano, Á.; Barriga-C., E.D.; Yate, L.; Ziolo, R.F. Enhanced Antibacterial activity of melt processed poly(propylene) Ag and Cu nanocomposites by argon plasma treatment. *Plasma Process. Polym.,* **2014**, *11*, 353-365.

[22] Martínez-Castañón, G.A.; Niño-Martínez, N.; Martínez-Gutierrez, F.; Martínez-Mendoza, J.R.; Ruiz, F. Synthesis and antibacterial activity of silver nanoparticles with different sizes. *J. Nanoparticle Res.,* **2008**, *10*, 1343-1348.

[23] Theivasanthi, T.; Alagar, M. X-Ray diffraction studies of copper nanopowder. *Arch. Phy. Res*., **2010**, *1*(2), 112-117.

[24] Hunter, R.C.; Beveridge, T.J. High-resolution visualization of *Pseudomonas aeruginosa* PAO1 biofilms by freeze-substitution transmission electron microscopy. *J. Bacteriol.,* **2005**, *187*, 7619-7630.

[25] Walters, M.C.; Roe, F.; Bugnicourt, A.; Franklin, M.J.; Stewart, P.S. Contributions of antibiotic penetration, oxygen limitation, and low metabolic activity to tolerance of *Pseudomonas aeruginosa* biofilms to ciprofloxacin and tobramycin. *Antimicrob. Agents Chemother.,* **2003**, *47*, 317-323.

[26] Odzak, N.; Kistler, D.; Behra, R.; Sigg, L. Dissolution of metal and metal oxide nanoparticles in aqueous media. *Environ. Pollut.,* **2014**, *191*, 132-138.

[27] Ehrlich, H.L. Microbes and metals. *Appl. Microbiol. Biotechnol.,* **1997**, *48*, 687-692.

[28] Salton, M.R.J. Studies of the bacterial cell wall. *Biochim. Biophys. Acta,* **1953**, *10*, 512-523.

[29] de Sousa Borges, A.; Scheffers, D.-J. Bacterial dynamin as a membrane puncture repair kit. *Environ. Microbiol.,* **2016**, *18*, 2298-2301.

[30] Ren, G.; Hu, D.; Cheng, E.W.C.; Vargas-Reus, M.A.; Reip, P.; Allaker, R.P. Characterisation of copper oxide nanoparticles for antimicrobial applications. *Int. J. Antimicrob. Agents,* **2009**, *33*, 587-590.

[31] Azam, A.; Ahmed, A.S.; Oves, M.; Khan, M.S.; Habib, S.S.; Memic, A. Antimicrobial activity of metal oxide nanoparticles against gram-positive and gram-negative bacteria: A comparative study. *Int. J. Nanomed.,* **2012**, *7*, 6003-6009.

[32] Raffi, M.; Mehrwan, S.; Bhatti, T.M.; Akhter, J.I.; Hameed, A.; Yawar, W.; ul Hasan, M.M. Investigations into the antibacterial behavior of copper nanoparticles against *Escherichia coli*. *Ann. Microbiol.,* **2010**, *60*, 75-80.

[33] Xu, X.-H.N.; Brownlow, W.J.; Kyriacou, S.V; Wan, Q.; Viola, J.J. Real-time probing of membrane transport in living microbial cells using single nanoparticle optics and living cell imaging. *Biochemistry,* **2004**, *43*, 10400-10413.

[34] Nour El Din, S.; El-Tayeb, T.A.; Abou-Aisha, K.; El-Azizi, M. *In vitro* and *in vivo* antimicrobial activity of combined therapy of

silver nanoparticles and visible blue light against *Pseudomonas aeruginosa*. *Int. J. Nanomed.,* **2016**, *11*, 1749-1158.

[35] Sondi, I.; Salopek-Sondi, B. Silver nanoparticles as antimicrobial agent: A case study on *E. coli* as a model for gram-negative bacteria. *J. Colloid Interface Sci.,* **2004**, *275*, 177-182.

[36] Ahmad, R.; Mohsin, M.; Ahmad, T.; Sardar, M. Alpha amylase assisted synthesis of TiO_2 nanoparticles: Structural characterization and application as antibacterial agents. *J. Hazard. Mater.,* **2015**, *283*, 171-177.

[37] Lee, Y.-J.; Kim, J.; Oh, J.; Bae, S.; Lee, S.; Hong, I.S.; Kim, S.-H. Ion release kinetics and ecotoxicity effects of silver nanoparticles. *Environ. Toxicol. Chem.,* **2012**, *31*, 155-159.

[38] Liu, J.; Hurt, R.H. Ion release kinetics and particle persistence in aqueous nano-silver colloids. *Environ. Sci. Technol.,* **2010**, *44*, 2169-2175.

[39] Thill, A.; Zeyons, O.; Spalla, O.; Chauvat, F.; Rose, J.; Auffan, M.; Flank, A.M. Cytotoxicity of CeO_2 nanoparticles for *Escherichia coli*. Physico-chemical insight of the cytotoxicity mechanism. *Environ. Sci. Technol*., **2006**, *40*(19), 6151-6156.

[40] Perreault, F.; Samadani, M.; Dewez, D. Effect of soluble copper released from copper oxide nanoparticles solubilization on growth and photosynthetic processes of *Lemna gibba*. *Nanotoxicology,* **2014**, *8*, 374-382.

[41] Studer, A.M.; Limbach, L.K.; Duc, L.V.; Krumeich, F.; Athanassiou, E.K.; Gerber, L.C.; Moch, H.; Stark, W.J. Nanoparticle cytotoxicity depends on intracellular solubility: Comparison of stabilized copper metal and degradable copper oxide nanoparticles. *Toxicol. Lett.,* **2010**, *197*, 169-174.

[42] Fahmy, B.; Cormier, S.A. Copper oxide nanoparticles induce oxidative stress and cytotoxicity in airway epithelial cells. *Toxicol. Vitr.,* **2009**, *23*, 1365-1371.

[43] Li, W.-R.; Xie, X.-B.; Shi, Q.-S.; Zeng, H.-Y.; Ou-Yang, Y.-S.; Chen, Y.-B. Antibacterial activity and mechanism of silver nanoparticles on *Escherichia coli*. *Appl. Microbiol. Biotechnol.,* **2010**, *85*, 1115-1122.

[44] Feng, Q.L.; Wu, J.; Chen, G.Q.; Cui, F.Z.; Kim, T.N.; Kim, J.O. A mechanistic study of the antibacterial effect of silver ions on *Escherichia coli* and *Staphylococcus aureus*. *J. Biomed. Mater. Res.,* **2000**, *52*, 662-668.

[45] Patil, M.P.; Kim, G.-D. Eco-friendly approach for nanoparticles synthesis and mechanism behind antibacterial activity of silver and anticancer activity of gold nanoparticles. *Appl. Microbiol. Biotechnol.,* **2017**, *101*, 79-92.

[46] Morones, J.R.; Elechiguerra, J.L.; Camacho, A.; Holt, K.; Kouri, J.B.; Ramírez, J.T.; Yacaman, M.J. The bactericidal effect of silver nanoparticles. *Nanotechnology,* **2005**, *16*, 2346-2353.

[47] Zeyons, O.; Thill, A.; Chauvat, F.; Menguy, N.; Cassier-Chauvat, C.; Oréar, C.; Daraspe, J.; Auffan, M.; Rose, J.; Spalla, O. Direct and indirect CeO_2 nanoparticles toxicity for *Escherichia coli* and *synechocystis*. *Nanotoxicology,* **2009**, *3*, 284-295.

[48] Le Ouay, B.; Stellacci, F. Antibacterial activity of silver nanoparticles: A surface science insight. *Nano Today,* **2015**, *10*, 339-354.

[49] Franci, G.; Falanga, A.; Galdiero, S.; Palomba, L.; Rai, M.; Morelli, G.; Galdiero, M. Silver nanoparticles as potential antibacterial agents. *Molecules,* **2015**, *20*, 8856-8874.

[50] Kiss, T.; Osipenko, O. Metal ion-induced permeability changes in cell membranes: A minireview. *Cell. Mol. Neurobiol.,* **1994**, *14*, 781-789.

[51] Dibrov, P.; Dzioba, J.; Gosink, K.K.; Häse, C.C. Chemiosmotic mechanism of antimicrobial activity of Ag(+) in *Vibrio cholerae*. *Antimicrob. Agents Chemother.,* **2002**, *46*, 2668-2670.

[52] Zhao, J.; Wang, Z.; Dai, Y.; Xing, B. Mitigation of CuO nanoparticle-induced bacterial membrane damage by dissolved organic matter. *Water Res.,* **2013**, *47*, 4169-4178.